Acta Crystallographica Section F
Structural Biology Communications
ISSN 2053-230X

Structures of adenosine kinase from *Trypanosoma brucei brucei*

Jennifer Timm,[a] Dolores González-Pacanowska[b] and Keith S. Wilson[a]*

[a]Structural Biology Laboratory, Department of Chemistry, University of York, Heslington, York YO10 5DD, England, and [b]Instituto de Parasitología y Biomedicina 'López-Neyra', Consejo Superior de Investigaciones Científicas, 18100 Armilla, Granada, Spain

Correspondence e-mail: keith.wilson@york.ac.uk

Received 7 November 2013
Accepted 12 December 2013

PDB references: apo *Tb*AK, 4n08; *Tb*AK–adenosine–AMPPNP, 4n09

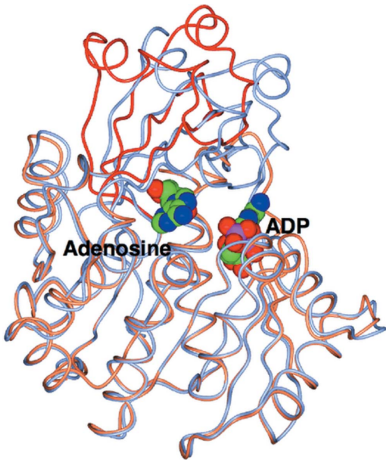

Trypanosoma brucei is a single-cellular parasite of the genus Kinetoplastida and is the causative agent of African sleeping sickness in humans. Adenosine kinase is a key enzyme in the purine-salvage pathway, phosphorylating adenosine to AMP, and also activates cytotoxic analogues such as cordycepin and Ara-A by their phosphorylation. The structures of *T. brucei brucei* adenosine kinase (*Tb*AK) in its unliganded open conformation and complexed with adenosine and ADP in the closed conformation are both reported to 2.6 Å resolution. The structures give insight into the binding mode of the substrates and the conformational change induced upon substrate binding. This information can be used to guide the improvement of cytotoxic substrate analogues as potential antitrypanosomal drugs.

1. Introduction

Parasites of the genus *Trypanosoma* cause a variety of devastating diseases, mainly in developing countries. *T. brucei* is the causative agent of African sleeping sickness (World Health Organization, 2011). All four current drugs show severe toxicity, and in addition resistance is emerging, so new chemotherapeutic agents are urgently needed and novel targets for drug development need to be identified (Barrett *et al.*, 2007). A key requirement is to identify major differences in the biochemical pathways between trypanosomes and their human hosts. One important difference lies in purine metabolism, since while mammalian cells are able to synthesize purines *de novo*, trypanosomes lack this ability and depend entirely on the purine-salvage pathway (el Kouni, 2003; James & Born, 1980). A key enzyme in the purine-salvage pathway is adenosine kinase (AK; Vodnala *et al.*, 2008), which catalyses the phosphorylation of adenosine to AMP. AK appears to be non-essential for the growth of the parasites, but it activates several cytotoxic adenosine analogues such as cordycepin and Ara-A (Iovannisci & Ullman, 1984). However, a major problem with these compounds as drug candidates is their degradation by adenosine deaminase *in vivo* (Mäser *et al.*, 2001; Williamson, 1972). If this limitation could be evaded by modifications of these compounds that hamper deamination yet do not alter their phosphorylation by AK, they could become candidates for the design of effective antitrypanosomal chemotherapeutics.

AK belongs to the phosphofructokinase B family of carbohydrate kinases, with two characteristic sequence motifs: the di-glycine switch close to the N-terminus and the sequence D*X*NGAGD close to the C-terminus (Park & Gupta, 2008). AKs of several species, including that of *T. brucei rhodesiense* (*Tb*AK; Kuettel *et al.*, 2011), have been well characterized. A number of crystal structures are known, which confirm that the enzymes have an open apoenzyme form but a closed form in complex with ligands and substrates (Cook *et al.*, 2000; Kuettel *et al.*, 2011; Mathews *et al.*, 1998; Muchmore *et al.*, 2006; Reddy *et al.*, 2007; Schumacher *et al.*, 2000; Zhang *et al.*, 2006, 2007). Here, we report the structures of *Tb*AK in the apo form and in complex with adenosine and adenosine diphosphate (*Tb*AK–adenosine–ADP). We show these to be very similar to the published structures of complexes with the activator (*Tb*AK–KRM) and the AP5A bi-substrate mimic (*Tb*AK–AP5A), respectively (Kuettel *et al.*, 2011).

2. Methods

2.1. Cloning, expression and purification

The gene coding for *Tb*AK (SwissProt entry Q584S0) was inserted into the YSBLIC3C vector using ligation-independent cloning (Fogg & Wilkinson, 2008). The construct included an N-terminal hexahistidine tag together with a cleavage site for HRV 3C protease. The cloning was confirmed by colony PCR and sequencing, and the construct was transformed into C41 cells and plated on Luria–Bertani plates containing 35 µg ml^{-1} kanamycin. The next day, the colonies were washed off with 5 ml Luria–Bertani medium and used for the inoculation of 8 × 500 ml medium. Cells were grown at 37°C with shaking at 180 rev min^{-1} (Innova 44, New Brunswick Scientific) until they reached an optical density at 600 nm of 0.2, and were then transferred to 20°C with shaking at 251 rev min^{-1}. Protein expression was induced by the addition of 1 m*M* isopropyl *β*-D-1-thiogalactopyranoside (IPTG) at an optical density at 600 nm of 0.6 for 6 h. The cells were harvested by centrifugation at 5000*g* for 30 min and washed with 100 ml PBS prior to freezing.

The cells were thawed on ice and were lysed in 80 ml lysis buffer *A* (20 m*M* Tris pH 7.5, 200 m*M* NaCl, 30 m*M* imidazole, 10 m*M* *β*-mercaptoethanol, 100 µ*M* PMSF) or buffer *B* (20 m*M* Tris pH 7.5, 200 m*M* NaCl, 30 m*M* imidazole, 1 m*M* DTT) using sonication. Cell debris was removed by centrifugation at 5000*g* and 4°C for 40 min. The supernatant was loaded onto a pre-equilibrated 5 ml HisTrap FF crude column (GE Healthcare), which was then washed with three column volumes of lysis buffer. The protein was eluted using an imidazole gradient. Protein-containing fractions were pooled and concentrated to ∼2 mg ml^{-1} before the addition of HRV 3C protease at a ratio of 1:100 protease:*Tb*AK. Proteolysis was monitored by 12% SDS–PAGE and had reached completion overnight at 4°C.

To remove the histidine tag and noncleaved *Tb*AK, the protein buffer was exchanged into lysis buffer using centrifugal filters (Amicon Ultra Centrifugal Filter from Millipore or Vivaspin 6 from Sartorium Stedim Biotech; 30 kDa cutoff) and nickel-affinity purification was performed using the same buffers as before. The resulting protein was concentrated and loaded onto a Superdex 75 column (GE Healthcare) in buffer consisting of 10 m*M* Tris pH 7.5, 200 m*M* NaCl with 10 m*M* *β*-mercaptoethanol or 1 m*M* DTT as reducing agent. The protein was concentrated to 96 mg ml^{-1}, dialyzed against the size-exclusion chromatography buffer, frozen in liquid nitrogen and stored at −80°C at a concentration of 48 mg ml^{-1}. Its identity was confirmed by electrospray ionization mass spectrometry.

Dynamic light-scattering experiments were carried out using a DynaPro (Protein Solutions) to determine the polydispersity of the samples before crystallization. For this, the protein was diluted to a concentration of 3 mg ml^{-1} at 20°C with a sample volume of 20 µl.

2.2. Crystallization

Crystallization proved to be challenging, with severe problems with regard to reproducibility. Screening was carried out using a Mosquito robot (TTP LabTech, UK) with sitting drops composed of 150 nl protein solution at a concentration of 30 mg ml^{-1} plus an equal volume of precipitant. For the complex, protein purified with buffers containing *β*-mercaptoethanol was screened in the presence of 1 m*M* adenosine and 1 m*M* *β*,*γ*-imidoadenosine 5′-triphosphate (AMPPNP). Crystals were optimized using hanging-drop vapour diffusion and the best crystals grew in 0.1 *M* bis-tris propane pH 8.5, 0.2 *M* sodium citrate, 24%(*w*/*v*) polyethylene glycol 3350 within three weeks to maximum dimensions of ∼600 × 100 × 50 µm.

For the apoenzyme, extensive screening failed to produce any crystals. Following the publication of the structure in the open form (Kuettel *et al.*, 2011), we focused around the conditions reported therein, using a protein sample purified with buffers containing DTT. This led to a large number of crystals, of which 200 were tested for diffraction. However, very few showed any diffraction, and finally only one provided a usable diffraction pattern, with the rest showing very restricted resolution or substantial splitting and disorder. The single usable crystal grew at 4°C in 0.1 *M* Tris pH 8.8, 60%(*v*/*v*) MPD, and grew to a maximum size of approximately 80 × 20 × 20 µm after one week.

Thus, the reducing agent appeared to affect the crystallization behaviour, as the protein purified with *β*-mercaptoethanol crystallized only in the closed conformation (with ligands added), whereas that purified in the presence of DTT crystallized only in the open conformation (without ligands). Furthermore, repeating the purification with the same or with modified buffer conditions failed to yield diffracting crystals even after extensive screening. It is relevant that Kuettel and coworkers were unable to obtain a well diffracting crystal of the apoenzyme (Kuettel *et al.*, 2011). In addition, extensive attempts to crystallize *Tb*AK in the presence of cordycepin or the transition-state analogues ADP–AlF_4–adenosine and ADP–MgF_4–adenosine were also unsuccessful.

2.3. Data collection, structure solution and refinement

Computations were performed using programs from the *CCP*4 suite (Winn *et al.*, 2011) unless otherwise stated. Data were processed using *XDS* (Kabsch, 2010*a*,*b*), *POINTLESS* (Evans, 2011) and *SCALA* (Evans, 2006). The crystal grown in the presence of adenosine and AMPPNP was cryoprotected in mother liquor containing 5% ethylene glycol and data were collected on beamline I24 at the Diamond Light Source (DLS). The crystal belonged to space group *C*2 with four molecules in the asymmetric unit. The unit-cell parameters do not allow twinning.

The apo crystal was not cryoprotected before vitrification and data were collected on beamline I03 at DLS. The crystal appeared to

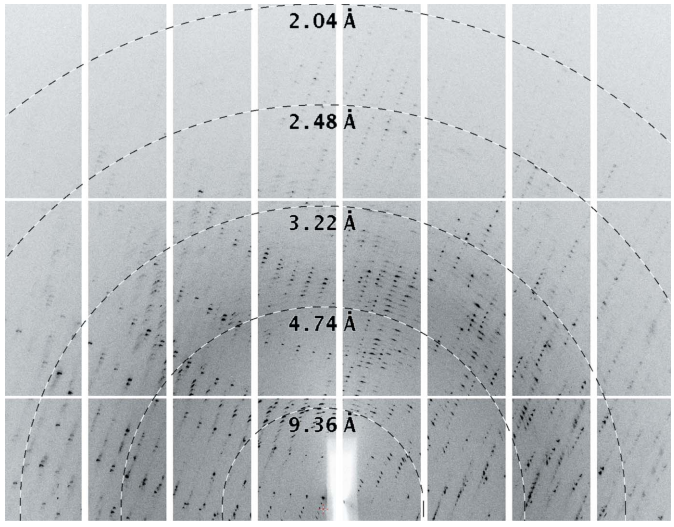

Figure 1
Diffraction pattern from the apo crystal of *Tb*AK. The figure shows a close-up of one of the images used for structure solution, with the rings annotating the resolution created using the *adxv* software (Arvai, 2012). The crystal is clearly split, with more than one lattice evident in the image. While the data appear to extend beyond 2.6 Å resolution on this image, the diffraction was anisotropic and the integration was restricted to 2.6 Å resolution overall.

Table 1
Crystallographic data and refinement statistics.

	Apo *Tb*AK	*Tb*AK–adenosine–AMPPNP
Data collection		
Diffraction source	DLS beamline I03	DLS beamline I24
Wavelength (Å)	0.9763	0.9686
Temperature (K)	100	100
Detector	Pilatus 6M-F	Pilatus 6M Prosport+
Rotation range per image (°)	0.2	0.2
Total rotation range (°)	180	220
Crystal data		
Space group	$P4_12_12$	$C2$
Unit-cell parameters		
a (Å)	60.08	184.53
b (Å)	60.08	90.22
c (Å)	192.86	98.04
α (°)	90.00	90.00
β (°)	90.00	103.78
γ (°)	90.00	90.00
Resolution (Å)	57.36–2.60 (2.74–2.60)	95.21–2.60 (2.74–2.60)
Total reflections	132048 (20863)	160133 (23793)
Unique reflections	11649 (1664)	47962 (6973)
Completeness (%)	99.90 (100)	99.5 (99.4)
Multiplicity	11.3 (12.5)	3.3 (3.4)
R_{merge}	0.120 (0.395)	0.176 (0.991)
$\langle I/\sigma(I)\rangle$	15.8 (6.3)	6.6 (2.3)
Matthews coefficient (Å^3 Da^{-1})	2.28	2.59
Refinement statistics		
Reflections, working set	10989	45507
Reflections, test set	660	2455
Resolution range (Å)	57.36–2.60	95.21–2.60
R factor	0.170	0.186
R_{free}	0.231	0.221
No. of non-H atoms		
Protein	2463	10276
Ligand	—	192
Water	157	148
Mean B factors (Å^2)		
Protein	38.0	45.2
Ligand	—	44.4
Water	40.5	38.3
R.m.s. deviation from ideal		
Bond lengths (Å)	0.013	0.012
Bond angles (°)	1.466	1.531
Ramachandran plot† (%)		
Residues in favoured region	93.6	96.05
Residues in allowed region	5.8	3.58
Outliers	0.6	0.37
MolProbity score	1.35	1.45
Poor rotamers‡ (%)	1.61	2.01
PDB code	4n08	4n09

† The Ramachandran plot was generated with *Coot* (Emsley *et al.*, 2010). ‡ Poor rotamer analysis was performed using *MolProbity* (Chen *et al.*, 2010).

consist of several independent lattices (Fig. 1), which limited the data quality. *XDS* selected one of these lattices and the data were integrated to 2.6 Å resolution in space group $P4_12_12$ with one molecule per asymmetric unit. As expected, the unit-cell parameters are closely similar to those reported for the KRM-soaked crystal by Kuettel and coworkers (PDB entry 2xtb; a = 61.24, c = 193.85 Å, also in space group $P4_12_12$). Analysis during data reduction clearly indicated that the crystal was not twinned, which was confirmed by the low R factors achieved during subsequent refinement in *REFMAC* (Murshudov *et al.*, 2011). The data and statistics for both crystals are summarized in Table 1.

The structures were solved by molecular replacement using *Phaser* (McCoy, 2007). At the time, human AK (PDB entry 1bx4; Mathews *et al.*, 1998), with a protein sequence identity of 40%, showed the highest homology to *Tb*AK and was used as the search model for *Tb*AK–adenosine–ADP. For apo *Tb*AK, the structure of *Tb*AK–KRM was used. Refinement was carried out using *REFMAC*5 (Murshudov *et al.*, 2011) with automatically generated local NCS restraints, and the model was rebuilt with *Coot* (Emsley *et al.*, 2010) and validated using *MolProbity* (Chen *et al.*, 2010).

3. Results and discussion

3.1. Characterization and crystallization

*Tb*AK was initially purified using buffers containing β-mercaptoethanol (BME) and PMSF for protease inhibition, but characterization by dynamic light scattering (DLS) revealed a polydispersity of approximately 75%. Analysis by ESI-MS showed peaks of 80 and 156 Da higher than that expected, which could be the result of phosphorylation (80 Da), a BME adduct (76 Da) or a PMSF adduct (156 Da). This batch led to crystals of *Tb*AK in the presence of adenosine and AMPPNP that diffracted to 2.6 Å resolution with four *Tb*AK molecules in the asymmetric unit. All four chains had clear density for both adenosine moieties and the α- and β-phosphates, but no density for a γ-phosphate. This could reflect high flexibility of the γ-phosphate owing to the lack of a coordinating Mg^{2+} ion, but is most likely to be the result of slow hydrolysis. We therefore modelled the ligand as ADP. No molecules of BME or PMSF were visible in the structure.

In a second protein preparation, the buffers were changed to avoid possible BME and PMSF adducts. DLS showed the protein to be monodisperse (10% polydispersity) and ESI-MS indicated a single species with a molecular weight of 38 187 Da (expected value of 38 184 Da). However, attempts to obtain new *Tb*AK–adenosine–AMPPNP crystals failed, as did attempts to obtain co-crystals with cordycepin or with magnesium and aluminium fluoride plus nucleotides. At this point, the structures of *Tb*AK in complex with the bi-substrate analogue diadenosine pentaphosphate (AP5A) and the activator 4-[5-(4-phenoxyphenyl)-2*H*-pyrazol-3-yl]morpholine (KRM) were published (Kuettel *et al.*, 2011). Using these conditions, we obtained a single apo crystal which diffracted to 2.6 Å resolution in space group $P4_12_12$ with one *Tb*AK per asymmetric unit, although the data quality was limited by the presence of more than one lattice.

3.2. Overall fold

The *T. brucei brucei* AK structure is highly similar to that of the enzyme from a closely related subspecies, *T. brucei rhodesiense* (Kuettel *et al.*, 2011), which has an identical amino-acid sequence, with the gene only differing by two silent mutations. It has only minor differences from those from *Anopheles gambiae* (*Ag*AK), human (*Hsa*AK), *Toxoplasma gondii* (*Tgo*AK) and *Mycobacterium tuberculosis* (*Mtu*AK) (Cook *et al.*, 2000; Mathews *et al.*, 1998; Muchmore *et al.*, 2006; Schumacher *et al.*, 2000; Zhang *et al.*, 2006, 2007). In brief, *Tb*AK consists of two domains: a large ATP-binding domain and a small lid domain. As in other eukaryotic AK structures, the larger domain consists of a typical α/β structure with a central nine-stranded β-sheet (β1, β5, β6, β9, β10, β11, β12, β13 and β14) enclosed by ten α-helices (α3–α12). The lid domain consists of a five-stranded β-sheet (β2, β3, β4, β7 and β8) at the interface to the large domain and two α-helices (α1 and α2) on top of it. The active site is located at the interface of the two domains.

The apo structure is in the open conformation, essentially identical to that reported for *Tb*AK soaked with the activator KRM (PDB entry 2xtb; Kuettel *et al.*, 2011) and that of apo *Tgo*AK (Schumacher *et al.*, 2000). Comparison with 2xtb showed that the overall structures are effectively the same, with the only differences being in the flexible loop region (residues 281–297). In addition, the activator complex is slightly more open, but this may not directly reflect the binding of the activator but may rather be an artefact of crystallization. The side chain of Leu138, close to the activator, has a different position in the two structures but makes no direct or indirect interactions with the activator itself.

3.3. Substrate binding

There are four independent protein molecules in the asymmetric unit, with well defined density for both the adenosine and for ADP (Fig. 2*a*). The four chains are closely similar: the r.m.s. between all C^{α} atoms is 0.37, 0.39 and 0.29 Å for chains *B*, *C* and *D* superposed on chain *A* using *SSM* (Krissinel & Henrick, 2004). Chain *A* is therefore used in the rest of the discussion and in the other panels of the figure.

*Tb*AK adopts a closed conformation similar to all other structures of complexes of AK with substrates or substrate analogues in both of the binding pockets of the active site. Superposition of the structures

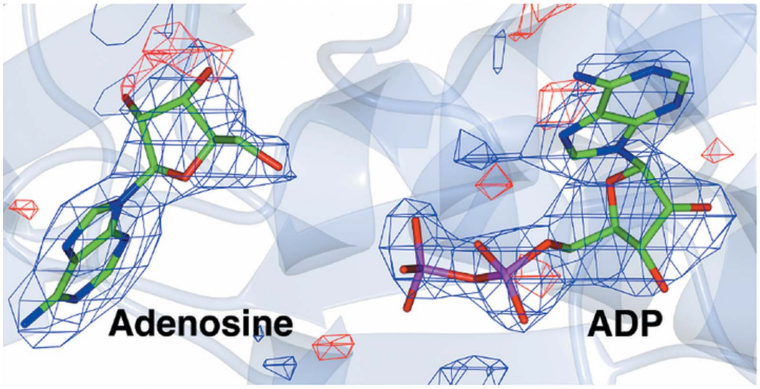

(*a*)

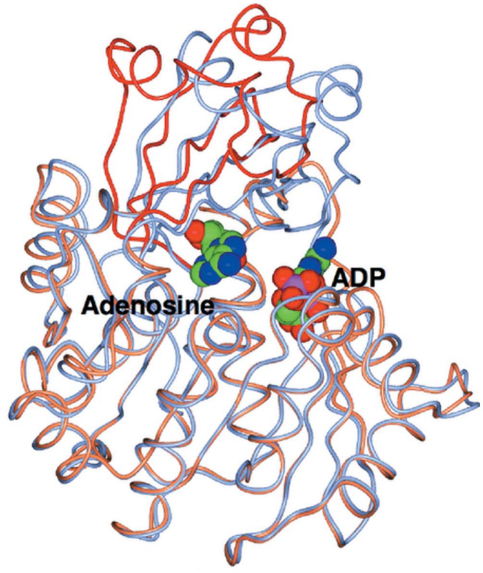

(*b*)

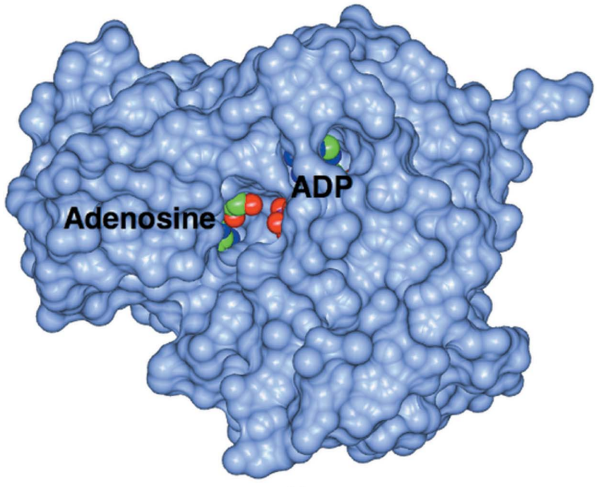

(*c*)

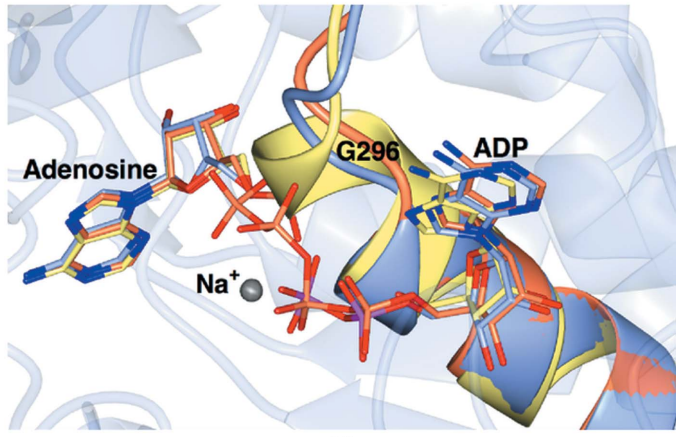

(*d*)

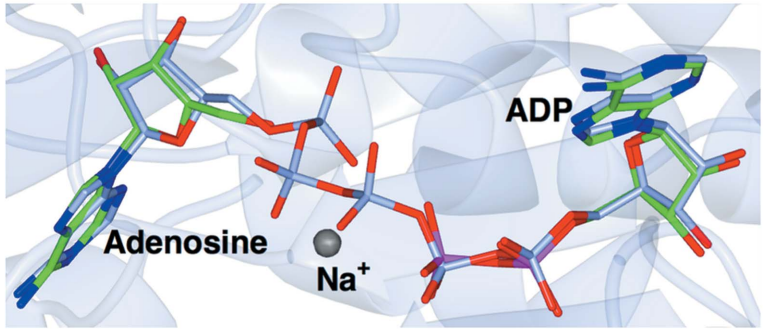

(*e*)

Figure 2
The structure of *Tb*AK. The views are all of the *A* chain, but there is essentially no difference between the four molecules in the asymmetric unit. (*a*) The unbiased maximum-likelihood difference map calculated with *REFMAC5* output coefficients contoured at 3σ before the ligands were added to the model. The positive contour is in blue and the negative contour is in red. The protein chain is shown as a semi-transparent ribbon. (*b*) Worm representations of the fold of the open apo form (coral core subunit and red lid) superposed on the closed form (ice blue). The structures were superposed using *SSM* (Krissinel & Henrick, 2004) based on the core subunit. The adenosine and ADP ligands are shown as spheres. (*c*) Surface view of the *A* chain, in which the two adenines can be seen to be buried in deep pockets. (*d*) Superposition of the anion-hole region of the *Tb*AK–adenosine–ADP complex (ice blue; the protein was co-crystallized with AMPPNP, which is presumed to have hydrolysed) reported here with those of *Tb*AK–AP5A (PDB entry 3otx, coral; Kuettel *et al.*, 2011) and human AK in complex with two adenosines (PDB entry 1bx4, lemon; Mathews *et al.*, 1998). The structures were superposed using *SSM* based on the C^{α} atoms in chain *A* of both. The ligands are shown as cylinders, with the C and P atoms coloured according to chain for clarity. (*e*) Superposition of *Tb*AK–adenosine–ADP with *Tb*AK–AP5A (PDB entry 3otx). The ribbon shows the *Tb*AK–adenosine–ADP trace. The ligands are shown as cylinders coloured as in (*d*). This figure was made with *CCP4mg* (McNicholas *et al.*, 2011).

of *Tb*AK in its closed and open forms using the *ProSMART* program in *REFMAC* (Murshudov *et al.*, 2011) confirmed that the smaller lid domain closes over the active site and the large domain contracts slightly (Fig. 2*b*). This results from a rigid-body rotation of 28° with hinge motions of the amino acids connecting the two domains. In addition, *Tb*AK undergoes smaller structural rearrangements while binding to and orienting its substrates. The adenosine makes hydrogen bonds to residues Asp13, Asp17, Gly62, Asn67, Asp299 (adenosine) and Asn222, Thr264, Thr270, His266, Gly298 and Gln288 (ADP), and stacking interactions of its adenine ring with Phe169 which align the helix adjacent to it. The interaction with the substrates causes a slight bending of the α12 helix (residues 318–330) and a closing of the loop (residues 266–268) near the ATP-binding site towards the ADP. These smaller movements orient the substrates in the binding pockets and bury the two adenine moieties (Fig. 2*c*).

Important for catalysis in nucleotide kinases is the anion hole (Schumacher *et al.*, 2000), a conserved sequence of residues essential for appropriate binding of the phosphates of the substrate, the formation of which requires the P-loop (residues 290–300) to be pushed outwards. The superposition of our structure of *Tb*AK–adenosine–ADP on those of *Tb*AK–AP5A and *Hsa*AK in complex with two adenosines shows it to be in an intermediate state between the latter two conformations, reflecting the importance of this motif (Fig. 2*d*). In our complex, the γ-phosphate of AMPPNP (which mimics the phosphate donor ATP) is missing, so that its interactions cannot help to arrange the loop completely, which is therefore not bent outwards as far as it would be with all three phosphates present. The structure of *Tb*AK–AP5A (Kuettel *et al.*, 2011) shows a fully developed anion hole; the complex of *Hsa*AK with two adenosines (Mathews *et al.*, 1998) lacks the anion-hole motif completely and instead has an extended α11 helix, as there are no phosphates in the active site. In particular, residues 294–298 (centred around Gly296) adopt a helical conformation in the absence of phosphate ligands, but change to a loop producing the anion hole when phosphates are present.

The structure of *Tb*AK–adenosine–ADP in the closed conformation was very similar to that of the complex with the bi-substrate analogue, *Tb*AK–AP5A (Kuettel *et al.*, 2011), with an r.m.s. on C^{α} positions of 0.57 Å (Fig. 2*e*). The adenines in both structures occupy essentially identical positions, as does the ribose of ADP and AP5A. In the *Tb*AK–AP5A complex there are five phosphates between the two adenosine moieties, two more than must be present in the transition state, so the phosphates would need to be in different conformations in the Michaelis complex and the transition state. Structures of adenylate kinase from *Aquifex aeolicus* have been determined in complex with both AP5A (PDB entry 2rgx; Henzler-Wildman *et al.*, 2007) and with the phosphoryl-transfer transition-state mimic ADP–AlF_4–AMP in the active site (PDB entry 3sr0; Y.-J. Cho & D. Kern, unpublished work). The enzyme was in a very similar closed conformation in both, suggesting that the enzyme conformation and the adenine-binding sites in the AP5A analogues were indeed representative of the true ligand-binding state. We therefore carried out extensive crystallization screens with nucleotides and magnesium and aluminium fluorides with the aim of obtaining a better mimic of the transition state. Unfortunately, none of these led to crystals of diffraction quality.

4. Conclusions

Crystallization of *Tb*AK proved to be surprisingly challenging given the substantial number of homologous structures in the PDB. Only one crystal, of limited quality, of the apoenzyme was identified and this provided diffraction data to 2.6 Å resolution, which were sufficient to allow a description of the enzyme in its open conformation. It is impressive that modern integration software can extract useful data from such a crystal.

The structure of *Tb*AK–adenosine–ADP was in the closed conformation and was very similar to that reported for the complex with the transition-state mimic, *Tb*AK–AP5A (Kuettel *et al.*, 2011). The two structures were superposed with an r.m.s.d. on C^{α} positions of 0.57 Å using *SSM* and the ligands are shown for chain *A* of both structures in Fig. 2(*e*). It is evident that the adenines in both structures occupy essentially identical positions, as does the ribose of ADP and AP5A. What is most notable about the *Tb*AK–AP5A complex is that there are five phosphates between two adenosine moieties, two more than must be present in the transition state. This indicates that the phosphates would need to be in different conformations in the Michaelis complex and the transition state, perhaps in part reflecting the absence of chelating metal in the present complex. Structural studies of adenylate kinase from *A. aeolicus* have yielded complexes of the enzyme with both AP5A (PDB entry 2rgx; Henzler-Wildman *et al.*, 2007) and with the phosphoryl-transfer transition-state mimic ADP–AlF_4–AMP in the active site (PDB entry 3sr0; Y.-J. Cho & D. Kern, unpublished work). In this system, the enzyme was in a very similar closed conformation in both structures, suggesting that the enzyme conformation and the adenine-binding sites in the AP5A analogues were indeed representative of the true ligand-binding state. However, extensive crystallization screens with nucleotides and magnesium and aluminium fluorides failed to produce useful crystals. One problem may lie in the fact that the aluminium fluoride in *Tb*AK would be coordinated by a phosphate O atom on one side and a ribose O atom on the other, unlike the adenylate kinase system, in which the aluminium is coordinated by phosphate O atoms on both sides. This requires further work.

We thank the Diamond Light Source (beamlines I24 and I03) for the provision of X-ray data-collection facilities. This work was funded by the European Union (grant agreement No. 223238).

References

Arvai, A. (2012). *adxv: A Program to Display X-ray Diffraction Images*. http://www.scripps.edu/~arvai/adxv.html.
Barrett, M. P., Boykin, D. W., Brun, R. & Tidwell, R. R. (2007). *Br. J. Pharmacol.* **152**, 1155–1171.
Chen, V. B., Arendall, W. B., Headd, J. J., Keedy, D. A., Immormino, R. M., Kapral, G. J., Murray, L. W., Richardson, J. S. & Richardson, D. C. (2010). *Acta Cryst.* D**66**, 12–21.
Cook, W. J., DeLucas, L. J. & Chattopadhyay, D. (2000). *Protein Sci.* **9**, 704–712.
Emsley, P., Lohkamp, B., Scott, W. G. & Cowtan, K. (2010). *Acta Cryst.* D**66**, 486–501.
Evans, P. (2006). *Acta Cryst.* D**62**, 72–82.
Evans, P. R. (2011). *Acta Cryst.* D**67**, 282–292.
Fogg, M. J. & Wilkinson, A. J. (2008). *Biochem. Soc. Trans.* **36**, 771–775.
Henzler-Wildman, K. A., Thai, V., Lei, M., Ott, M., Wolf-Watz, M., Fenn, T., Pozharski, E., Wilson, M. A., Petsko, G. A., Karplus, M., Hübner, C. G. & Kern, D. (2007). *Nature (London)*, **450**, 838–844.
Iovannisci, D. M. & Ullman, B. (1984). *Mol. Biochem. Parasitol.* **12**, 139–151.
James, D. M. & Born, G. V. (1980). *Parasitology*, **81**, 383–393.
Kabsch, W. (2010*a*). *Acta Cryst.* D**66**, 125–132.
Kabsch, W. (2010*b*). *Acta Cryst.* D**66**, 133–144.
Kouni, M. H. el (2003). *Pharmacol. Ther.* **99**, 283–309.
Krissinel, E. & Henrick, K. (2004). *Acta Cryst.* D**60**, 2256–2268.
Kuettel, S., Greenwald, J., Kostrewa, D., Ahmed, S., Scapozza, L. & Perozzo, R. (2011). *PLoS Negl. Trop. Dis.* **5**, e1164.
Mäser, P., Vogel, D., Schmid, C., Räz, B. & Kaminsky, R. (2001). *J. Mol. Med.* **79**, 121–127.

Mathews, I. I., Erion, M. D. & Ealick, S. E. (1998). *Biochemistry*, **37**, 15607–15620.
McCoy, A. J. (2007). *Acta Cryst.* D**63**, 32–41.
McNicholas, S., Potterton, E., Wilson, K. S. & Noble, M. E. M. (2011). *Acta Cryst.* D**67**, 386–394.
Muchmore, S. W., Smith, R. A., Stewart, A. O., Cowart, M. D., Gomtsyan, A., Matulenko, M. A., Yu, H., Severin, J. M., Bhagwat, S. S., Lee, C. H., Kowaluk, E. A., Jarvis, M. F. & Jakob, C. L. (2006). *J. Med. Chem.* **49**, 6726–6731.
Murshudov, G. N., Skubák, P., Lebedev, A. A., Pannu, N. S., Steiner, R. A., Nicholls, R. A., Winn, M. D., Long, F. & Vagin, A. A. (2011). *Acta Cryst.* D**67**, 355–367.
Park, J. & Gupta, R. S. (2008). *Cell. Mol. Life Sci.* **65**, 2875–2896.
Reddy, M. C., Palaninathan, S. K., Shetty, N. D., Owen, J. L., Watson, M. D. & Sacchettini, J. C. (2007). *J. Biol. Chem.* **282**, 27334–27342.
Schumacher, M. A., Scott, D. M., Mathews, I. I., Ealick, S. E., Roos, D. S., Ullman, B. & Brennan, R. G. (2000). *J. Mol. Biol.* **298**, 875–893.
Vodnala, M., Fijolek, A., Rofougaran, R., Mosimann, M., Mäser, P. & Hofer, A. (2008). *J. Biol. Chem.* **283**, 5380–5388.
Williamson, J. (1972). *Trans. R. Soc. Trop. Med. Hyg.* **66**, 354–355.
Winn, M. D. *et al.* (2011). *Acta Cryst.* D**67**, 235–242.
World Health Organisation (2011). *Trypanosomiasis Fact Sheet*. http://www.who.int/trypanosomiasis_african/en/.
Zhang, Y., el Kouni, M. H. & Ealick, S. E. (2006). *Acta Cryst.* D**62**, 140–145.
Zhang, Y., el Kouni, M. H. & Ealick, S. E. (2007). *Acta Cryst.* D**63**, 126–134.